

# Numerical models of hydromagnetic dynamos

By S. A. JEPPE

School of Mathematics and Physics, University of East Anglia,  
Norwich, England†

(Received 6 September 1973 and in revised form 5 April 1974)

The magnetic induction equation is solved numerically in a sphere for a variety of prescribed fluid flows. The models considered are the so-called ‘ $\alpha\omega$  dynamos’, in which both small-scale turbulence and large-scale shearing play a significant role. Solutions are obtained by marching the finite-difference equations forward in time from some initial field. For a critical value of the magnetic Reynolds number  $R_m$  solutions which neither grow nor decay are found.

Further calculations are performed with a ‘cut-off effect’ in which an attempt is made to simulate the effect of the Lorentz forces on the turbulence. For supercritical values of  $R_m$  the magnetic field now stabilizes at a finite value instead of increasing indefinitely. The form of the final field is compared with that produced at critical  $R_m$  in the absence of the cut-off effect.

---

## 1. Introduction

The study of the dynamo problem grew out of a desire to explain the mechanism by which the magnetic fields of the earth and sun are maintained. The problem consists of obtaining solutions of the magnetic induction equation and the equation of motion of the fluid material involved such that the magnetic field does not tend to zero with increasing time. Ideally the resulting magnetic fields should mimic those of the naturally occurring dynamos, both in spatial structure and variation with time. The fields of the earth and sun are similar in that they both resemble that of a dipole, but they differ in the nature of their time dependence. The magnetic field of the sun is oscillatory with a period of 22 years, whereas that of the earth remains virtually constant for periods of several thousands of years, interrupted by sudden, apparently random, reversals.

An additional feature of the solar field is the migration of the sunspot zones towards the equator in the course of each 11 year half-cycle. This phenomenon has been portrayed in the celebrated Butterfly Diagram of Maunder (1922). The sunspots are accompanied by magnetic fields of several thousand gauss, compared with a few gauss for the dipole field, revealing the presence of powerful azimuthal fields which predominate over the dipole component in the interior of the sun. This leads to the conclusion that the migration of the sunspot zones towards the equator is reflected in a similar migration of the zones in which the

† Present address: Mathematical Services Department, British Aircraft Corporation, Warton Aerodrome, Preston PR4 1AX, England.

azimuthal fields are strongest. The models considered herein offer an explanation for the time-dependent behaviour of the solar field, but give little insight into the nature of the geomagnetic reversals.

The two governing equations are coupled, a Lorentz term involving the magnetic field appearing in the equation of motion, and an induction term depending on the fluid velocity in the equation for the magnetic field. If a small magnetic field is assumed, however, the Lorentz force, being quadratic in the magnetic field strength, may be ignored. The equations then uncouple to the extent that the equation of motion can be solved first, and the solution substituted in the induction equation. The subsequent investigation of this latter equation has given rise to the so-called kinematic dynamo problem. It is in this direction that most of the existing work on dynamo theory has been directed, since the governing equation has the advantage of being linear.

In fact, the kinematic dynamo problem can be regarded as one of linear stability, the object being to determine the conditions under which the state of zero magnetic field becomes unstable. Once such a state is reached, however, any small initial magnetic field will rapidly grow until the original small field assumption is invalidated. It may then be argued that in practice the ignored Lorentz force must modify the velocity field, reducing its capacity to regenerate the magnetic field, until at a certain magnetic field strength a balance is reached, the field just being maintained against ohmic losses.

The full fluid-mechanical problem is nonlinear, and has received comparatively little attention in view of the difficulties experienced with the apparently far simpler kinematic case. These difficulties are highlighted by the presence of non-existence theorems, which prohibit the existence of dynamos possessing convenient symmetrical structures. The most far reaching of these results was proved by Cowling (1933), and precludes the possibility of an axially symmetric magnetic field sustained by dynamo action. Any model put forward as a possible dynamo must therefore be fully three-dimensional. Attempts to solve the kinematic problem in a sphere for non-axisymmetric velocities produced a series of models all of which proved incapable of sustaining a magnetic field. An account of these may be found in papers by Bullard & Gellman (1954), Lilley (1970) and Gibson & Roberts (1969). Success has, however, been achieved by Gubbins (1972), who chose axisymmetric velocities. The magnetic fields generated by the Gubbins model are not, however, axisymmetric, since Cowling's theorem would then preclude dynamo action. Unfortunately the possibility of formulating a fully magnetohydrodynamic model in which the velocity field is axisymmetric must be ruled out, as only a particularly fortuitous choice of body force could enable the axial symmetry of the flow field to be maintained against the necessarily asymmetric Lorentz forces.

A major development in dynamo theory was made by Steenbeck, Krause & Rädler (1966), a translation of which together with later work by the same authors has been prepared by Roberts & Stix (1971). By considering the statistical properties of turbulent motion, they argued that turbulence in which there was a lack of mirror symmetry had the effect of inducing a large-scale electric current parallel to the applied magnetic field. This phenomenon, termed

the  $\alpha$ -effect, simplifies the problem considerably, since the large-scale fields can be assumed to be axisymmetric. There is now no question of Cowling's theorem precluding dynamo action, since the small-scale fields are non-axisymmetric. In the case of the earth or sun, the requisite lack of mirror symmetry is provided by the rotation of these bodies, which induces a similar lack of symmetry, or 'helicity', into the turbulence via the Coriolis forces. The models considered in the present paper will all make use of the  $\alpha$ -effect.

The task of determining the criterion for marginal stability in the kinematic case is an eigenvalue problem, in which various eigenvalues of the magnetic Reynolds number correspond to different eigenfunctions for the magnetic field. The eigenfunction corresponding to the smallest eigenvalue represents the most easily excited dynamo mode. The method of solving this problem in the past has been to use a combination of orthogonal-function expansions and finite-difference methods to reduce it to a matrix eigenvalue problem, which can then be solved numerically. Here we use a different technique in which the unsteady form of the induction equation is represented by finite differences and marched forward in time from some initial condition. This method, which enables the development of the magnetic field from the initial 'seed' field to be followed, allows nonlinear effects of the type described below to be incorporated into the model. It was also anticipated that it would largely forestall the convergence problems which have sometimes arisen with the eigenvalue problem.

The effect of Lorentz forces for situations in which the magnetic Reynolds number exceeds its critical value will be modelled in the following way. As with kinematic models of turbulent dynamos, the distribution of the  $\alpha$ -effect and the large-scale flow will be prescribed. Instead of the  $\alpha$ -effect at a fixed point remaining constant, however, we shall take it to be a function of the magnetic field strength at that point. For the field strength to stabilize as in naturally occurring dynamos, we must choose a decreasing function here. The choice of a suitable function is discussed further in §5. The actual effect of the Lorentz forces is, of course, far more complicated, and may be expected to modify the large-scale flow field as well as the turbulence. The marching technique described here could, in principle, be extended to include such a phenomenon, although the exact nature of this effect is not known. A more sophisticated formulation must await further developments in the field of turbulent magnetohydrodynamics.

## 2. The governing equations

The models investigated in this paper assume a sphere of homogeneous electrically conducting fluid surrounded by an insulating medium which extends to infinity. The governing equation for the large-scale magnetic field  $\mathbf{B}$  inside this sphere is

$$\partial\mathbf{B}/\partial t = R_\omega \text{curl}(\mathbf{U} \times \mathbf{B}) + R_\alpha \text{curl}(\alpha\mathbf{B}) + \nabla^2\mathbf{B}, \quad (2.1)$$

where  $\mathbf{U}$  is the large-scale fluid velocity. The second term on the right-hand side represents the contribution to the field due to the  $\alpha$ -effect. In the above equation the variables representing the velocity and  $\alpha$ -effect have been non-dimensional-

ized with respect to typical magnitudes  $U^*$  and  $\alpha^*$  of these quantities. Distance is measured in units of  $L$ , the radius of the sphere. The dimensionless parameters

$$R_\omega = U^*L/\eta, \quad R_\alpha = \alpha^*L/\eta$$

are magnetic Reynolds numbers based on the large-scale motion and  $\alpha$ -effect respectively, where  $\eta$  is the magnetic diffusivity.  $t$  is measured in units of a typical diffusion time  $L^2/\eta$ .

It will be assumed throughout that, with the exception of the small-scale turbulent motions, the system is axisymmetric. The magnetic and velocity fields can then each be written as the sum of an azimuthal (toroidal) and meridional (poloidal) part. Thus

$$\mathbf{B} = b\mathbf{1}_\phi + \text{curl}(a\mathbf{1}_\phi), \quad (2.2)$$

$$\mathbf{U} = u\mathbf{1}_\phi + \text{curl}(v\mathbf{1}_\phi). \quad (2.3)$$

The meridional and azimuthal parts of (2.1) can then be equated separately (see Steenbeck & Krause 1969) to yield

$$(\partial a/\partial t)\mathbf{1}_\phi = R_\omega(\text{curl } v\mathbf{1}_\phi \times \text{curl } a\mathbf{1}_\phi) + R_\alpha\alpha b\mathbf{1}_\phi + \nabla^2(a\mathbf{1}_\phi), \quad (2.4)$$

$$(\partial b/\partial t)\mathbf{1}_\phi = R_\omega \text{curl}\{u\mathbf{1}_\phi \times \text{curl } a\mathbf{1}_\phi + \text{curl } v\mathbf{1}_\phi \times b\mathbf{1}_\phi\} + \nabla^2(b\mathbf{1}_\phi). \quad (2.5)$$

Here the creation of toroidal flux by the  $\alpha$ -effect has been ignored. As mentioned in the introduction, there is evidence that in the case of the solar field the toroidal component is far stronger than the poloidal. The same may possibly be true of the earth. This suggests that differential rotation is the dominant mechanism in the creation of toroidal flux and is the basis for the above approximation.

Introducing a system of spherical co-ordinates (2.4) and (2.5) become

$$\partial a/\partial t = (E + F)a + R_\alpha\alpha b, \quad (2.6)$$

$$\partial b/\partial t = (E - F)b + R_\omega Ga, \quad (2.7)$$

where  $E$  and  $G$  are the linear operators

$$E = \frac{\partial^2}{\partial r^2} + \left\{ \frac{2}{r} - \frac{R_\omega}{r \sin \theta} \frac{\partial}{\partial \theta} (v \sin \theta) \right\} \frac{\partial}{\partial r} + \frac{1}{r^2} \frac{\partial^2}{\partial \theta^2} + \left\{ \frac{R_\omega}{r^2} \frac{\partial}{\partial r} (rv) + \frac{\cot \theta}{r^2} \right\} \frac{\partial}{\partial \theta} - \frac{1}{r^2 \sin^2 \theta}, \quad (2.8)$$

$$G = \left\{ \frac{u \cot \theta}{r} - \frac{1}{r} \frac{\partial u}{\partial \theta} \right\} \frac{\partial}{\partial r} + \left\{ \frac{1}{r} \frac{\partial u}{\partial r} - \frac{u}{r^2} \right\} \frac{\partial}{\partial \theta} + \left\{ \frac{\cot \theta}{r} \frac{\partial u}{\partial r} - \frac{1}{r^2} \frac{\partial u}{\partial \theta} \right\}, \quad (2.9)$$

and  $F$  is given by

$$F = R_\omega \left( \frac{\cot \theta}{r} \frac{\partial v}{\partial r} - \frac{1}{r^2} \frac{\partial v}{\partial \theta} \right). \quad (2.10)$$

Although the physical magnitude of the toroidal magnetic field is far greater than that of the meridional component, it is computationally convenient for the variables representing them to have the same order of magnitude. To this end we make the transformation

$$a = (R_\alpha/R_\omega)^{\frac{1}{2}} a', \quad b = (R_\omega/R_\alpha)^{\frac{1}{2}} b'. \quad (2.11)$$

Equations (2.6) and (2.7) then become

$$\partial a' / \partial t = (E + F)a' + R_m \alpha b', \quad (2.12)$$

$$\partial b' / \partial t = (E - F)b' + R_m G a', \quad (2.13)$$

where

$$R_m = (R_\alpha R_\omega)^{\frac{1}{2}}.$$

In the absence of meridional circulation ( $v = 0$ ), only one dimensionless parameter appears, the magnetic Reynolds number  $R_m$ . In future, use of the transformed variables will be assumed, and the primes omitted.

Outside the sphere we have

$$\text{curl}^2 (a \mathbf{1}_\phi) = 0. \quad (2.14)$$

In spherical polar co-ordinates this becomes

$$\frac{\partial^2 a}{\partial r^2} + \frac{2}{r} \frac{\partial a}{\partial r} + \frac{1}{r^2} \frac{\partial^2 a}{\partial \theta^2} + \frac{\cot \theta}{r^2} \frac{\partial a}{\partial \theta} - \frac{a}{r^2 \sin^2 \theta} = 0. \quad (2.15)$$

The boundary condition at the surface  $r = 1$  can be shown to reduce to

$$[a] = [\partial a / \partial r] = [b] = 0, \quad (2.16)$$

where square brackets denote the jump in the enclosed quantity. At infinity the absence of external sources of magnetic field requires that

$$a \rightarrow 0 \quad \text{as} \quad r \rightarrow \infty. \quad (2.17)$$

Equations (2.12), (2.13) and (2.15), together with boundary conditions (2.16) and (2.17), form the mathematical model whose numerical solution is described below.

### 3. Numerical techniques

Since (2.12) and (2.13) are parabolic, they may be solved numerically by marching forward in time from a set of initial conditions. A spatial grid is introduced so that the derivatives of the dependent variables can be expressed in finite-difference form. Since we are dealing throughout with an axisymmetric situation, it is only necessary to consider a grid in the  $r, \theta$  plane.

It is physically realistic to assume that the large-scale velocity field has mirror symmetry about the equatorial plane. This implies that  $u$  is an even function of latitude, while  $v$  is an odd function. In addition the  $\alpha$ -effect is taken to be an odd function of latitude. This last assumption is justified in the geophysical and astrophysical context, since the Coriolis forces which give rise to the lack of mirror symmetry in the turbulence, and hence to the  $\alpha$ -effect, change sign at the equator.

Under these conditions an examination of the symmetry of the problem reveals that solutions for the magnetic field break down into two quite separate families, as has been noted by Roberts (1972). For one of these  $a$  is an even function of latitude and  $b$  an odd function. Such a field is said to have dipole symmetry. The second type has  $a$  odd and  $b$  even, and is said to have quadrupole symmetry. If the symmetry of the solution to be sought is decided in advance, it is only

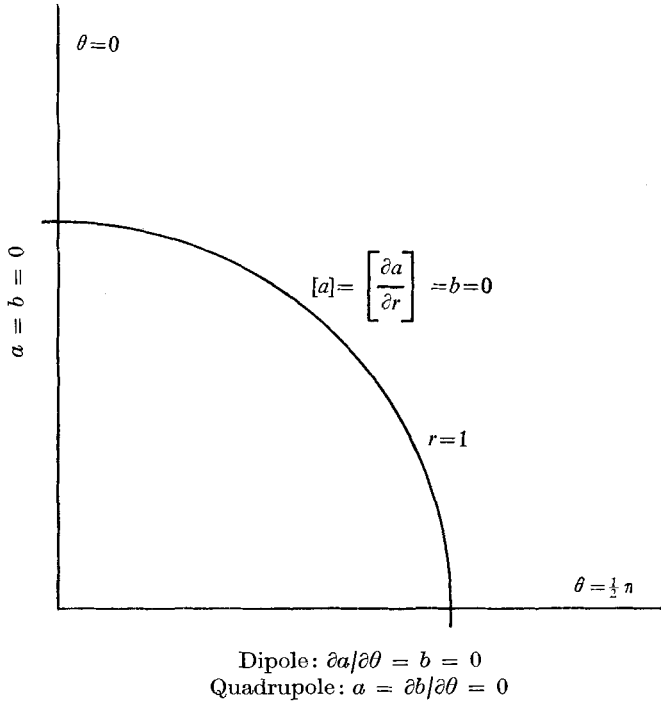


FIGURE 1. The region in which the governing equations (2.12), (2.13) and (2.15) are to be solved, showing the relevant boundary conditions.

necessary to consider the quadrant  $0 \leq \theta \leq \frac{1}{2}\pi$ . The nature of the required solution then determines the form of the boundary condition to be applied at  $\theta = \frac{1}{2}\pi$ .

The domains in which the governing equations are to be solved, together with the relevant boundary conditions, are shown in figure 1. The conditions at the boundaries  $r = 0$  and  $\theta = 0$  arise from the fact that  $a$  and  $b$  were originally the norms of azimuthal vectors. If they are to be both single valued and axisymmetric such vectors must vanish on the axis of symmetry.

For the numerical integration the scheme of Du Fort & Frankel (1953) was employed. Since this scheme involves three levels in time a simple forward-difference scheme was required to initiate the integration from a single set of initial conditions.

Of the boundary conditions shown in figure 1, the only one which presents any difficulty in the numerical solution of (2.12) and (2.13) is that which matches the internal and external values of  $a$  across the boundary  $r = 1$ . We are faced with the problem of simultaneously solving the parabolic equation (2.12), and (2.15), which is elliptic, in such a way that this condition is satisfied for all time.

A further complication arises from the fact that (2.15) has to be solved in an infinite domain. This latter obstacle can be removed by inversion. We write  $p(r) = a(1/r)$ . Equation (2.15) then becomes

$$r^2 \frac{\partial^2 p}{\partial r^2} + \frac{\partial^2 p}{\partial \theta^2} + \cot \theta \frac{\partial p}{\partial \theta} - \frac{p}{\sin^2 \theta} = 0, \tag{3.1}$$

which must now be solved on the inside of the sphere, enabling the same finite-difference mesh to be used as for the other two equations. The condition on  $a$  at infinity inverts to give the requirement that  $p$  be non-singular at the origin. The condition at  $r = 1$  becomes

$$\partial a / \partial r = -\partial p / \partial r, \quad a = p. \quad (3.2)$$

Using a three-point backward-difference approximation for the derivatives then yields the relation

$$p(1) = \frac{2}{3}\{a(1 - \Delta r) + p(1 - \Delta r)\} - \frac{1}{6}\{a(1 - 2\Delta r) + p(1 - 2\Delta r)\}. \quad (3.3)$$

An early version of the computer program achieved the simultaneous solution of (3.1) and (2.12) by carrying out the following series of operations at each time step. First of all the finite-difference forms of (2.12) and (2.13) were employed to find the values of  $a$  and  $b$  at all interior points at the next time level. Equation (3.1) was then solved iteratively, using a successive over-relaxation technique, to give  $p$  at all interior points. Relation (3.3) was used to recalculate the boundary values of  $p$  after each iteration. When sufficient convergence had been obtained, the values of  $a$  on  $r = 1$  were set equal to those of  $p$  in readiness for the next time step.

In later versions of the program a more efficient method was employed. The external field is of no interest in itself; it is merely used to find the boundary values of  $a$ , which then appear in the finite-difference expression for the interior values at the next time step. Denote the vector whose components are the values of  $a$  at boundary points by  $\mathbf{a}_B$ , and the vector consisting of the values of  $a$  at the two rows of points immediately inside the boundary by  $\mathbf{a}_I$ . The iterative procedure outlined above calculates the boundary values  $\mathbf{a}_B$  given  $\mathbf{a}_I$ . Since  $\mathbf{a}_B$  is a linear function of  $\mathbf{a}_I$ , there exists a matrix  $\mathbf{M}$  such that

$$\mathbf{M}\mathbf{a}_I = \mathbf{a}_B. \quad (3.4)$$

It is only necessary to calculate  $\mathbf{M}$  once at the start of the calculation. The boundary values of  $a$  can then be found at any subsequent time by means of a simple matrix multiplication. This latter method resulted in a reduction in computing time, in some cases by as much as a factor of three. The concept of using matrix multiplication to find the boundary values was suggested by a similar technique used by R. Thirlby (unpublished work) to apply the same boundary condition to a non-turbulent fluid-mechanical dynamo.

In practice a separate program was used to calculate  $\mathbf{M}$ , and output its elements on punched cards. The matrix was calculated column by column, using the fact that, if the iterative procedure described above is performed with the  $n$ th component of  $\mathbf{a}_I$  unity and all the other components zero, then the boundary values obtained consist of the  $n$ th column of the matrix  $\mathbf{M}$ .

For the nonlinear calculations, in which  $\alpha$  is a function of  $\mathbf{B}$ , one further operation was carried out at each time step; the new distribution of  $\alpha$  based on the current magnetic field was calculated. This distribution was then used for the next time step.

The calculations were performed on an ICL 1905E computer at the University of East Anglia. This machine has 64K words of  $1.8 \mu\text{s}$  store of which 21K are

available to the user. When using a spatial mesh of  $10 \times 10$  intervals, and calculating the boundary values by the matrix multiplication method, the computer time necessary to advance one time step was approximately 0.4 s. In addition several short 16 mm cine films of the solutions were made using an SC4020 graphics unit driven by an ICL1906A at the Atlas Computing Laboratory, Didcot.

#### 4. Linear models

The technique described above enables the development of the magnetic field to be investigated for any given choice of velocity field and  $\alpha$ -effect distribution. Attention has been confined, however, to three models which have been put forward by previous authors as exhibiting the basic features of naturally occurring dynamos. All three models feature a differential rotation in which the angular velocity is a function of depth alone, a rotation rate increasing with depth being anticipated from elementary considerations of angular-momentum conservation. There is evidence in the sun for a slight variation of angular velocity with latitude also, but it is doubtful whether this affects the basic dynamo action.

In this section the solutions for the linear case, that is, for  $\alpha$  independent of  $\mathbf{B}$ , are described and compared with the results obtained previously using the eigenvalue-problem approach. The effects of introducing nonlinearities into the models by making  $\alpha$  a function of  $\mathbf{B}$  are described in the next section. As a check on the accuracy of the integration scheme, an example of the induction of a toroidal magnetic field by the action of a differential rotation on a poloidal field was examined. A time-step length of 0.001 was used and ten grid points were taken in the  $r$  and  $\theta$  directions. The calculated magnetic field was plotted when the toroidal field strength was at its maximum, and a comparison with the analytic solution made. The discrepancy was barely discernible, suggesting that there would be little point in using a finer grid, except possibly for models with a complex spatial structure.

##### *Model 1*

The velocity field is specified by

$$\alpha = \frac{7.29}{16} r^3 (1 - r^2)^2 \cos \theta, \quad (4.1 a)$$

$$u = \pm \frac{19.683}{40.060} r (1 - r^2)^5 \sin \theta, \quad (4.1 b)$$

$$v = 0. \quad (4.1 c)$$

The eigenvalue problem for this model has been investigated by Roberts (1972). The constants have been chosen in such a way as to ensure that the absolute values of  $\alpha$  and the toroidal shearing  $\omega' = \partial(u/r \sin \theta)/\partial r$  have unit maxima. The negative sign in (4.1 *b*) corresponds to positive  $\omega'$  and vice versa. Reference to the governing equations (2.12) and (2.13) reveals that the system is unchanged if the signs of the  $\alpha$ -effect, differential rotation, and either part of the magnetic field are reversed simultaneously. The situation alters, however, if the sign of the product  $\alpha\omega'$  is reversed. Solutions of dipole and quadrupole type were sought for both positive and negative  $\alpha\omega'$ . In order that the magnitude of the solution should



Sign of $\alpha\omega'$	Symmetry	$R_m$	Frequency
+	Dipole	255	63.7 (66.4)
-	Dipole	210	47.4 (47.4)
+	Quadrupole	210	46.5 (49.7)
-	Quadrupole	255	62.8 (64.4)

TABLE 1

remain fairly constant throughout the integration, values of  $R_m$  close to the eigenvalues obtained by Roberts were used. The initial fields for this and the two subsequent models were taken to be the slowest decaying poloidal modes having the appropriate symmetry. This choice was arbitrary; there seems to be no reason to suspect that the subsequent development is particularly sensitive to the initial field distribution. As the integration proceeded the solutions rapidly settled down to give oscillatory 'dynamo wave' patterns similar to those predicted by the eigenvalue-problem approach. The frequency of these oscillations was estimated by counting the number of time steps needed to complete one cycle. The results are shown in table 1, with the values obtained by Roberts in parentheses.

It should be emphasized that for these calculations the magnetic Reynolds number  $R_m$  is a quantity to be prescribed in advance, rather than a result of the calculation. The long-term behaviour of the solution then indicates whether the specified value of  $R_m$  was above or below critical. In all cases the solutions for this model exhibited a gradual increase in intensity with time, demonstrating that the specified magnetic Reynolds numbers were slightly supercritical. No attempt was made to ascertain the exact critical value.

The evolution of the magnetic field for the two preferred modes, namely the dipole for  $\alpha\omega' < 0$  and the quadrupole for  $\alpha\omega' > 0$ , is shown in figures 2 and 3 respectively.

### Model 2

We now consider a model of the solar dynamo which was put forward by Steenbeck & Krause (1969). Both the differential rotation and  $\alpha$ -effect are confined to thin layers, their distributions being given by

$$\alpha = \frac{1}{2}\{1 + \operatorname{erf}[(r - r_2)/d]\} \cos \theta, \quad (4.2a)$$

$$u = \frac{1}{2}r\{1 - \operatorname{erf}[(r - r_1)/d]\} \sin \theta, \quad (4.2b)$$

$$v = 0. \quad (4.2c)$$

The shear layer in which the differential rotation takes place is centred at  $r = r_1$ , here taken to be 0.7, and the  $\alpha$ -effect is only significant outside a shell of radius  $r_2$ , taken to be 0.9. A value of 0.075 was used for  $d$ , a measure of the layer thickness. Steenbeck & Krause pursued the effect of making the layers thinner. In view of the difficulties inherent in applying finite-difference methods to models in which thin layers occur, attention was confined to the model as described above. Despite this, the mesh used for model 1 could hardly have been expected to yield

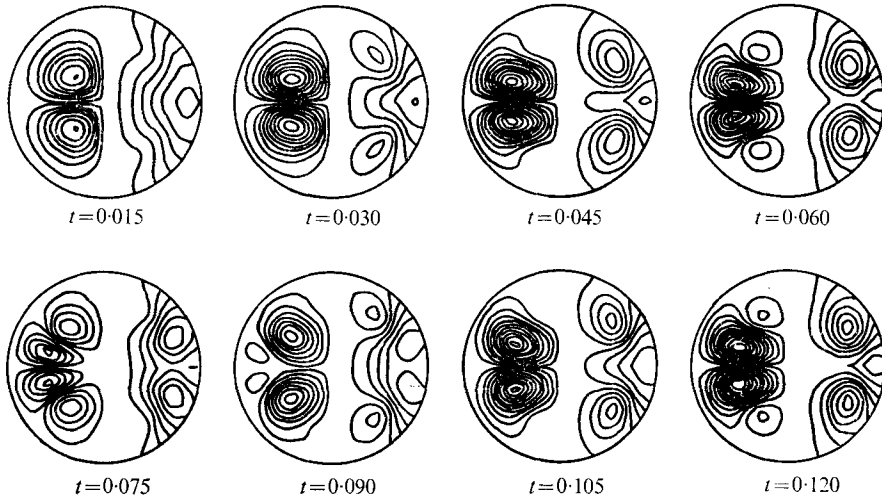


FIGURE 2. Evolution of the solution of dipole symmetry for model 1 with  $\alpha\omega' < 0$ . Each section shows contours of toroidal field strength on the left and poloidal field lines on the right. Here and in subsequent diagrams of this type, the first four pictures show the starting transient. The lower row represents approximately one half-cycle of the oscillation which repeats itself indefinitely for subsequent times. The migration of the field pattern from the poles to the equator is clearly discernible.

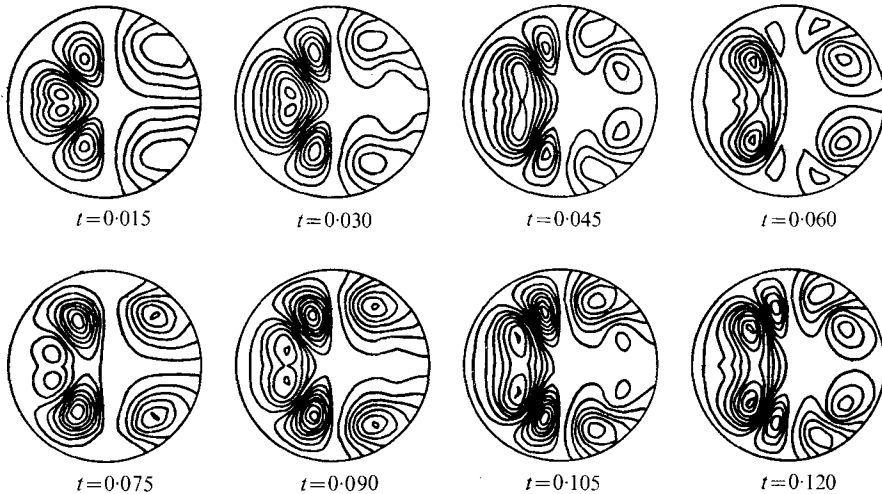


FIGURE 3. Evolution of the solution of quadrupole symmetry for model 1 with  $\alpha\omega' > 0$ . In this solution the direction of migration is from the equator to the poles. See also caption to figure 2.

accurate results, as the spacing between grid points is of the same order as the layer thickness. The number of grid points in the  $r$  direction was therefore increased to 20.

The evolution of the field having dipole symmetry is shown in figure 4. Steenbeck & Krause's eigenvalue of 144 was used as the magnetic Reynolds number. As with model 1, the solution rapidly attained a regular oscillatory state.

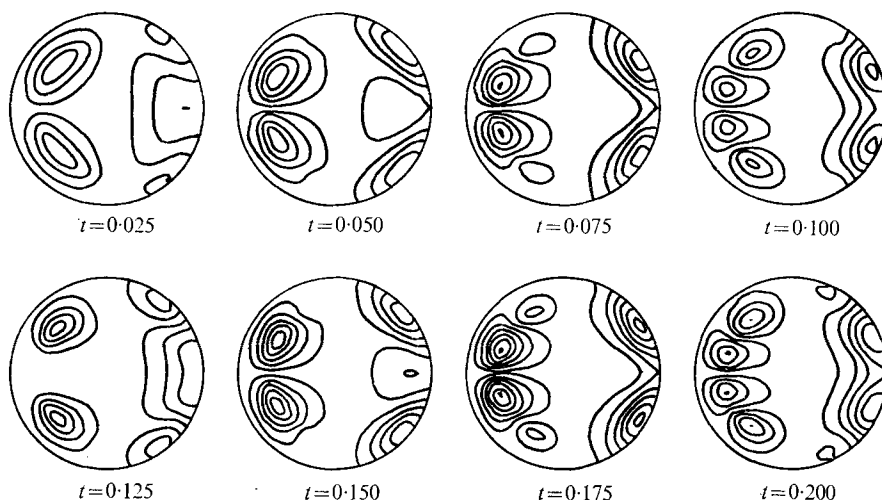


FIGURE 4. Evolution of the magnetic field for model 2 in the linear case with  $\alpha\omega' < 0$ . The direction of migration of the magnetic fields is from the poles to the equator. See also caption to figure 2.

The frequency of the oscillations was estimated at 32.2, which compares with the value of 31.8 obtained by Steenbeck & Krause. A more recent study of this model by Roberts & Stix (1972), using an alternative integration scheme, yielded a frequency of 31.6. One trial calculation for the quadrupole case, using the same value of  $R_m$ , was performed, the rapidly decaying solution confirming that the preferred solution does indeed possess dipole symmetry.

Figure 5 shows the butterfly diagram for this model. It is, in fact, a contour diagram of the toroidal field strength  $b$  at a radial distance  $r = 0.9$ , lines of constant  $b$  being plotted in the  $t, \theta$  plane. This diagram clearly illustrates the rapid adjustment of the solution from the initial state of zero toroidal field to the regular oscillatory state with zones of maximum toroidal field migrating from the poles to the equator. The steady growth in the amplitude of the oscillations indicates that the prescribed magnetic Reynolds number was slightly supercritical.

### Model 3

Model 3 differs from the previous two in that large-scale meridional circulations are present as well as differential rotation. It is defined by

$$\alpha = 24 \times 3^{\frac{1}{2}} r^2 (1-r)^2 \cos \theta \sin^2 \theta, \quad (4.3a)$$

$$u = \pm \frac{3}{8} \times 3^{\frac{1}{2}} r (1-r^2)^2 \sin \theta, \quad (4.3b)$$

$$v = \frac{7.168}{243} \times 2^{\frac{1}{2}} m r^5 (1-r)^2 \cos \theta \sin \theta. \quad (4.3c)$$

This model was put forward originally by Braginskii (1964) as representing the liquid core of the earth. Further calculations have been performed by Roberts, whose normalization we use here. As with model 1, the maxima of the azimuthal shearing and  $\alpha$ -effect are chosen to be unity, as is a typical meridional flow speed.

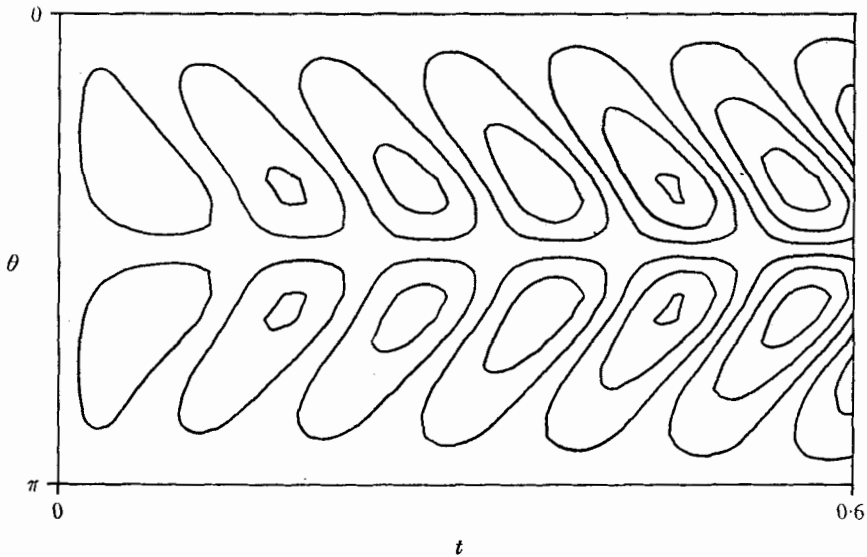


FIGURE 5. The butterfly diagram for the solution shown in figure 4. The curves are contours of constant toroidal field strength at  $r = 0.9$ . The migration towards the equator is clearly shown, while the gradual increase in field intensity with time indicates that the magnetic Reynolds number is slightly supercritical.

Sign of $\alpha\omega'$	Symmetry	$R_m$	Frequency	
			10 × 10 grid	20 × 20 grid
+	Dipole	113	80.6	89.2 (93.34)
-	Dipole	95	76.2	76.3 (77.35)
+	Quadrupole	95	69.9	73.9 (77.57)
-	Quadrupole	113	88.2	89.8 (93.54)

TABLE 2

In the absence of meridional circulation ( $m = 0$ ) this model produces an oscillatory magnetic field qualitatively similar to that of model 1. Numerical results for this model are shown in table 2.

Some of the results obtained using the 10 × 10 grid of model 1 differ considerably from Roberts' (shown in parentheses). This is probably because at frequencies of oscillation approaching 100 the electromagnetic skin depth is of the same order as the grid spacing. The calculations were therefore repeated using a 20 × 20 mesh, which produced more acceptable agreement. The solutions for this model in the case  $m = 0$  are qualitatively similar to those of the previous two, in that the preferred solution is an oscillatory dipole when  $\alpha\omega'$  is negative, corresponding to the positive sign in (4.3*b*), and an oscillatory quadrupole when  $\alpha\omega'$  is positive.

The situation for  $m \neq 0$  is fundamentally different. Roberts was able to show that for  $|m|$  sufficiently large the preferred solution was always steady. This

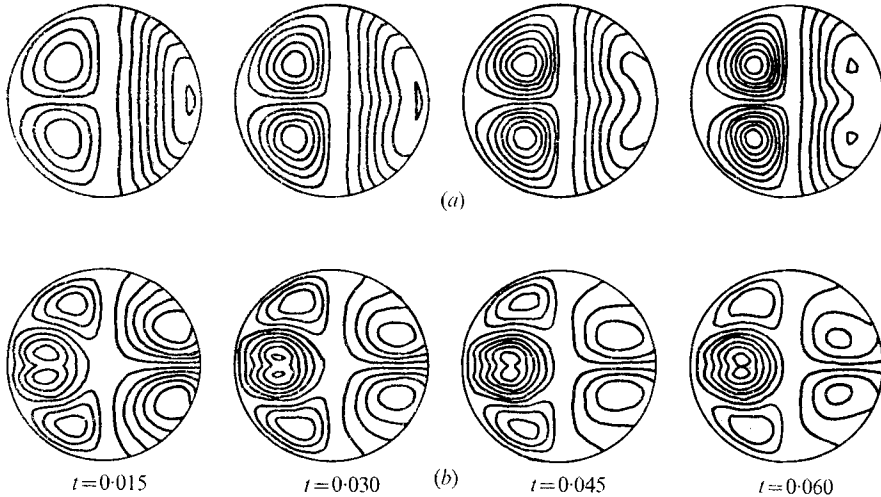


FIGURE 6. Evolution of the solutions of (a) dipole and (b) quadrupole symmetry for model 3 in the linear case. The sign of  $\alpha\omega'$  is positive in the dipole case; negative for the quadrupole. The meridional circulation is characterized by  $m = -0.15$  and  $m = 0.19$  respectively. The solutions are apparently tending towards the steady states found by Roberts (1972).

steady mode has the opposite symmetry to the corresponding oscillatory mode, a quadrupole now forming the preferred solution when  $\alpha\omega'$  is negative, and a dipole when  $\alpha\omega'$  is positive. There was in each case a value of  $m$  for which the dynamo was most efficient, the magnetic fields in these cases having a particularly simple spatial structure. These two cases were examined using the time-stepping technique. Figure 6 shows the evolution of these non-oscillatory solutions from the initial decay-mode field for values of  $m$  of  $-0.15$  and  $0.19$  for solutions of dipole and quadrupole symmetry respectively. The magnetic Reynolds number was specified as 43. The fields are apparently tending towards the steady-state solutions portrayed in Roberts (1972, figures 6*b, f*).

## 5. Nonlinear models

Having established that for linear models the time-stepping technique gives results in general agreement with those obtained from the eigenvalue problem, it was next decided to explore the possibility of making  $\alpha$  depend on the magnetic field strength. This was accomplished by introducing a revised measure of the  $\alpha$ -effect denoted by  $\hat{\alpha}$  and defined by

$$\hat{\alpha}(r, \theta, b) = P\alpha(r, \theta)/(1 + |b|^n). \quad (5.1)$$

This choice of cut-off law was not based on any analysis of the turbulence, and was chosen merely for simplicity. The use of the toroidal field strength  $|b|$  rather than the total field strength  $|\mathbf{B}|$  simplifies the computation and is compatible with the assumption made earlier that the magnetic field is predominantly toroidal. The quantity  $P$  gives a measure of the degree to which the magnetic Reynolds number is supercritical, the critical case corresponding to  $P = 1$ .

Models 2 and 3 of the previous section were investigated in this way.

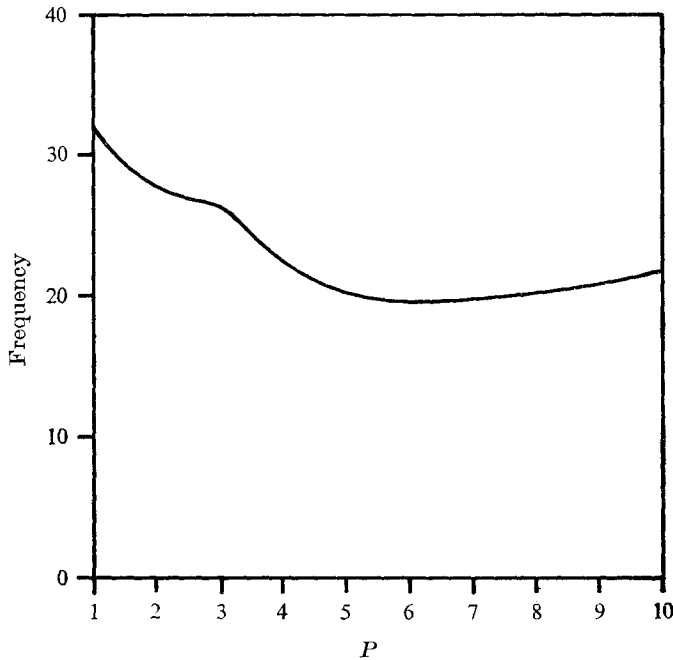


FIGURE 7. Frequency of oscillation plotted against the factor  $P$  by which the magnetic Reynolds number is supercritical for model 2 using Stix's cut-off law.

### *Model 2*

Three values for the parameter  $n$  in (5.1) were considered for this model, namely 1, 3 and the limiting case  $n \rightarrow \infty$ . The value  $n = 1$  is suggested by the fact that in many examples of classical magnetohydrodynamics, for example flow through a duct with an applied transverse magnetic field, the flow speed is inversely proportional to the magnetic field strength for large magnetic fields. It is slightly unrealistic for small fields, however, since it yields a cut-off law with discontinuous slope at  $b = 0$ . In one of the few papers to consider the full fluid-mechanical dynamo problem, Moffatt (1972) obtained the relation  $\alpha \sim M^{-\frac{1}{2}}$  for a certain choice of velocity field, where  $M$  is the magnetic energy. It was this result which prompted the investigation of the case  $n = 3$ . Finally, the limit  $n \rightarrow \infty$  corresponds to the cut-off law used by Stix (1972), in which the  $\alpha$ -effect is constant for field strengths less than some critical value, which may be taken to be unity, and zero for stronger fields.

Stix's investigations were confined to solutions of the induction equation which are functions of a single Cartesian co-ordinate only. Calculations for our spherical model were performed for a range of values of  $P$  from 1 to 10. Figure 7 shows the dependence of the oscillation frequency on the magnetic Reynolds number. The general agreement with Stix's results, in particular the reproduction of the minimum in the oscillation frequency near  $P = 7$ , appeared encouraging. Since the completion of these calculations, however, it has been asserted by Stix (private communication) that the position of this minimum is dependent on the

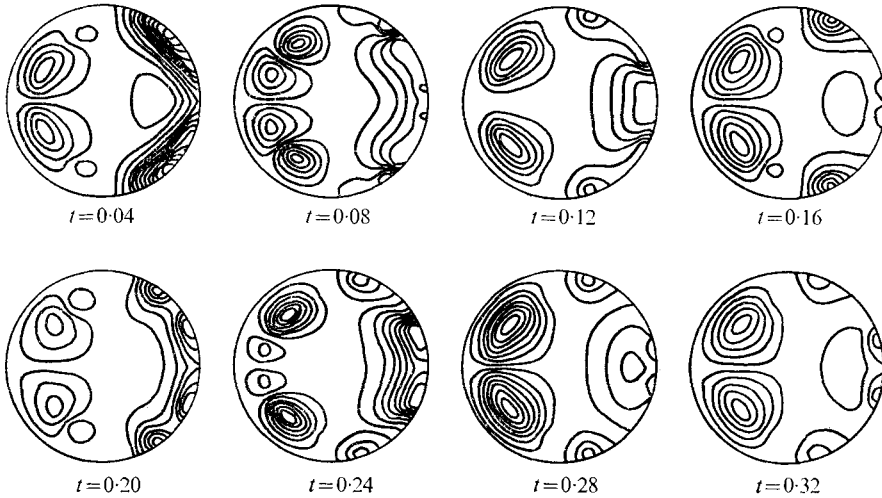


FIGURE 8. Evolution of the magnetic field for model 2 using Stix's cut-off law with  $P = 7$ . The distortion caused by the sharp cut-off of the  $\alpha$ -effect is evident, cf. figure 4.

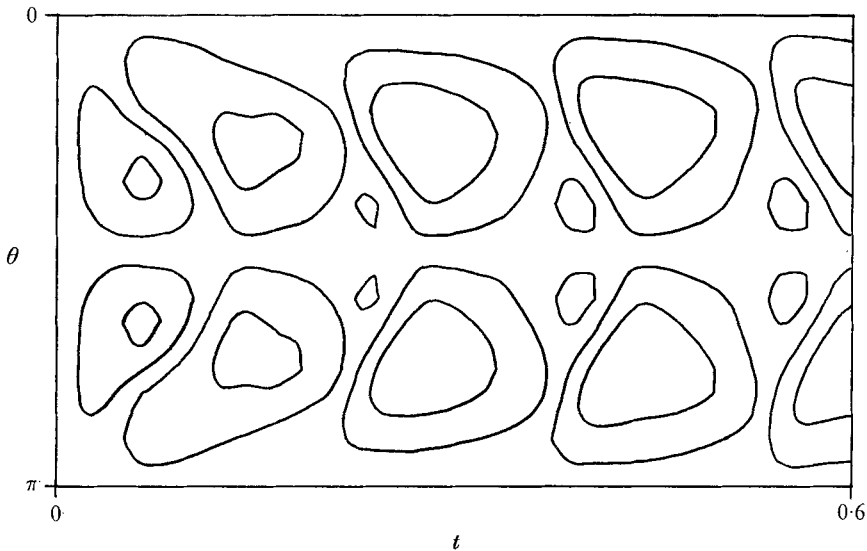


FIGURE 9. The butterfly diagram for the solution shown in figure 8. The migration towards the equator is less pronounced than for the linear model, cf. figure 5.

number of grid points taken. The author has not been able to determine whether or not his calculations for the spherical model also exhibit this property. If such were indeed the case one would be forced to conclude that the numerical scheme used, though satisfactory for linear models, does not adequately represent the governing equations in the nonlinear case. Solutions were attempted for  $P > 10$ , but the resulting fields failed to exhibit a regular time-dependent behaviour.

In contrast to the above results, the solutions for the case  $n = 1$  remained regular for large  $P$ , a range of values up to  $P = 100$  being considered. Figure 10

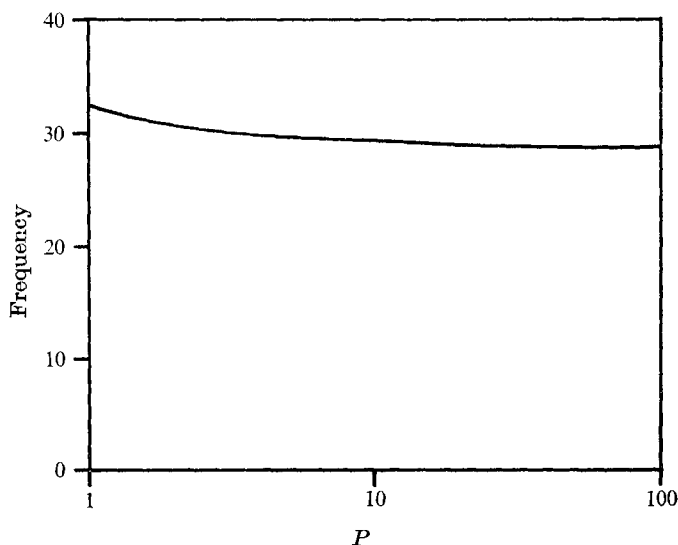


FIGURE 10. Frequency of oscillation plotted against the factor  $P$  by which the magnetic Reynolds number is supercritical for model 2 in the case  $n = 1$ .

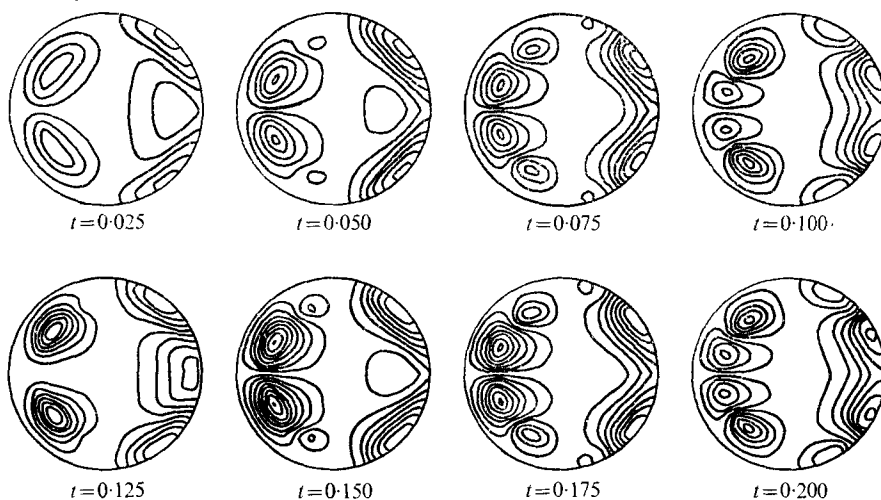


FIGURE 11. Evolution of the magnetic field for model 2 in the case  $n = 1$ ,  $P = 10$ . The gradual cut-off of the  $\alpha$ -effect causes far less distortion of the solution predicted by linear theory than does the abrupt cut-off law of Stix, cf. figures 4 and 8.

shows how the oscillation frequency is virtually independent of  $P$  for highly supercritical dynamos. The solution for  $P = 10$  is shown in figure 11. A comparison with figure 4 indicates that the solution is similar to that predicted by the linear theory.

Finally, the solutions for  $n = 3$  were calculated. For  $P \leq 10$  the solutions were not greatly different from those obtained for the linear problem. For more highly supercritical magnetic Reynolds numbers, however, the solutions exhibited a new feature not observed for the other two values of  $n$ . At the beginning of the integra-



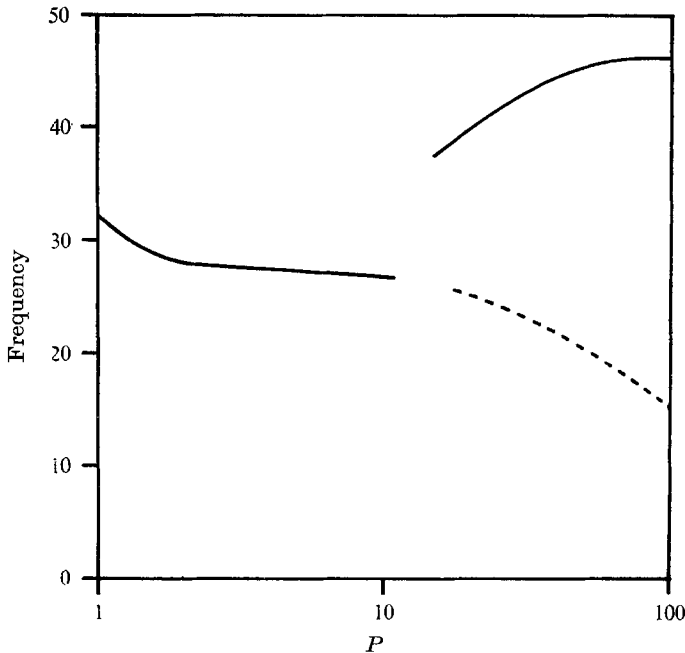


FIGURE 12. Frequency of oscillation plotted against the factor  $P$  by which the magnetic Reynolds number is supercritical for model 2 in the case  $n = 3$ . For high values of  $P$  a transition from a low frequency mode (broken curve) to a high frequency (solid curve) occurs after a few cycles.

tion, the solution assumed an oscillatory form with a frequency considerably below that of the linear model. The dynamo oscillated in this mode for a few cycles only, however. There then followed a transition to a mode of oscillation with a frequency higher than that of the linear model. This complete sequence of events can be observed in figure 13, which shows the butterfly diagram for the case  $P = 100$ . The difference between the frequencies of the two modes increases with  $P$  as may be seen from figure 12.

The use of an arbitrary cut-off law such as that defined by (5.1) leaves much to be desired. Ideally the dependence of the  $\alpha$ -effect on the magnetic field strength should be derived first, and then used in the computational model to attempt to predict the form of the solar magnetic field. In the absence of the magneto-hydrodynamic turbulence theory necessary to derive the true cut-off law, we may reverse the process, and by trying a variety of possible relations, obtain some insight into the form of the actual cut-off law which applies in the sun by comparing the resulting solutions with the observed solar field.

In the linear case this model reproduces well the migration of the sunspot zones portrayed in Maunder's original butterfly diagram. The two more abrupt cut-off laws, those with  $n = 3$  and  $n \rightarrow \infty$ , give considerable distortion of this pattern, especially when  $P$  is highly supercritical. We may therefore deduce that the actual process by which the  $\alpha$ -effect is reduced by the increasing Lorentz forces is a fairly gradual one, and is more closely modelled by  $n = 1$ .

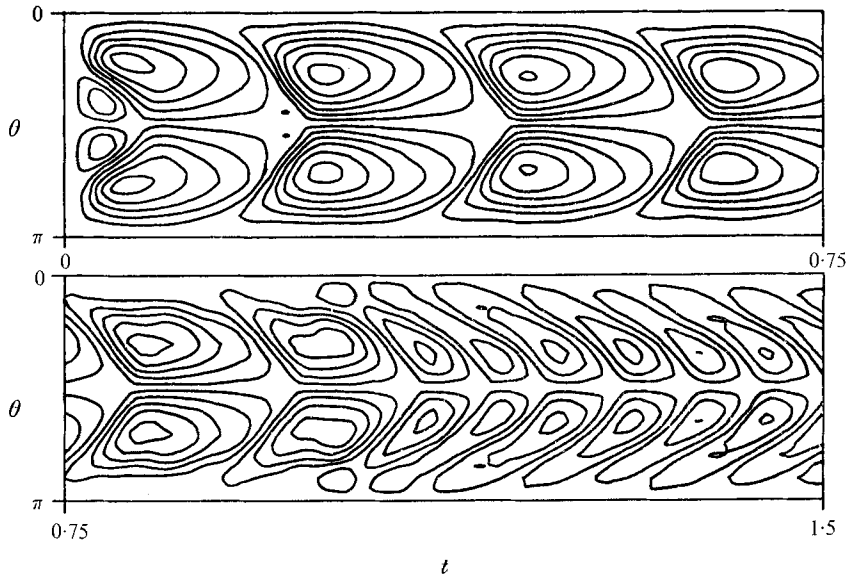


FIGURE 13. Butterfly diagram for model 2 for the case  $n = 3$ ,  $P = 100$ , showing the transition between low and high frequency modes of oscillation.

The sharp cut-off used by Stix is probably more appropriate to a non-rotating system, in which transition from a turbulent to a laminar flow regime may be expected as the magnetic field increases. In a rapidly rotating system, in which the Coriolis and Lorentz forces act in opposition, a different situation arises. The Coriolis forces tend to suppress turbulence, but are opposed in this by the Lorentz forces. It is therefore probable that the intensity of the turbulence actually increases with increasing magnetic field strength. However, since it is the Coriolis forces which give rise to helicity in the turbulence, the counteracting Lorentz forces can nevertheless bring about a reduction in the helicity, and hence in the  $\alpha$ -effect, as the magnetic field increases.

### Model 3

The results for model 2 showed that for the most gradual cut-off of the  $\alpha$ -effect, corresponding to the case  $n = 1$ , the effect of the nonlinearities was to stabilize the magnetic field in a form similar to that predicted by linear theory, even at very highly supercritical magnetic Reynolds numbers. Model 3 was investigated for the case  $n = 1$  to determine whether this result carried over to dynamos with meridional circulation. Attention was confined to the two cases  $m = -0.15$  and  $m = 0.19$ , for which steady modes are most easily excited. At  $P = 10$  it was found that there was now a fundamental difference between the solutions of dipole and quadrupole type. As might have been anticipated, the solution with dipole symmetry eventually assumed a form similar to the steady solution predicted by the linear theory. Somewhat unexpected, however, was the fact that in growing from a weak initial 'seed' field, the solution passed through an oscillatory phase, performing several oscillations before making the transition to

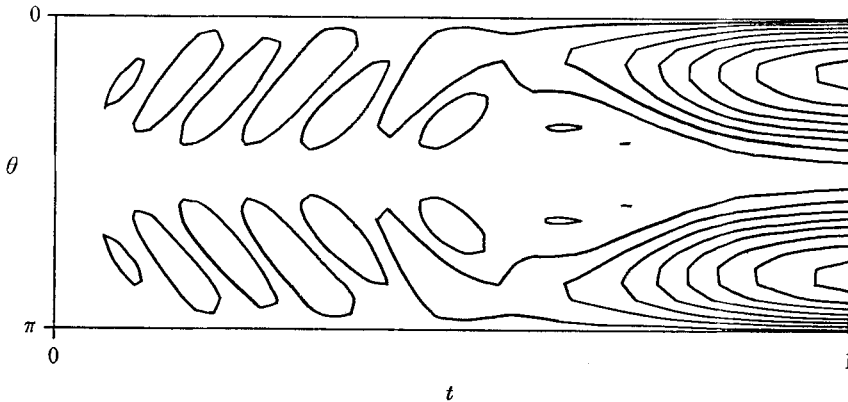


FIGURE 14. Butterfly diagram for the dipole-type solution of model 3 with  $n = 1$ ,  $P = 10$ ,  $m = -0.15$  and  $\alpha\omega' > 0$ . A transition from an oscillatory to a steady solution occurs after a few cycles of oscillation.

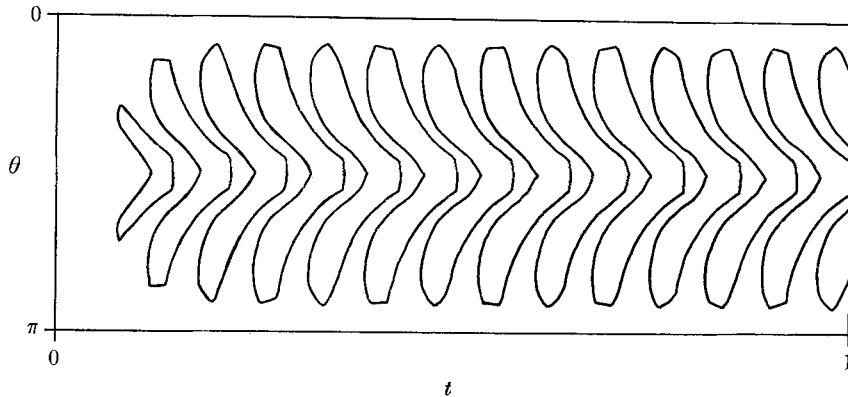


FIGURE 15. Butterfly diagram for the quadrupole-type solution of model 3 with  $n = 1$ ,  $P = 10$ ,  $m = 0.19$  and  $\alpha\omega' < 0$ . In contrast to the dipole-type solution (see figure 14) the oscillations apparently continue indefinitely.

a steady state. This behaviour is best illustrated by means of the butterfly diagram for this model, which is shown in figure 14.

For the quadrupole case, the solution also went into an oscillatory state initially. In this case, however, there was no transition to a steady state, the oscillations apparently continuing indefinitely. The butterfly diagram for this model is shown in figure 15.

An explanation for this behaviour can be found in the layer dynamo investigated analytically by Parker (1971). For a steady mode it was found that, as the magnetic Reynolds number is increased past its critical value, the growth rate at first grows towards a positive maximum, and then declines, eventually becoming negative. For the steady mode to be preferred in Parker's model the layer thickness has to be large, in which case it is difficult to envisage the model being distorted into a sphere. However, if one is prepared to accept that meridional circulation is equivalent to a large layer thickness to the extent that it causes the

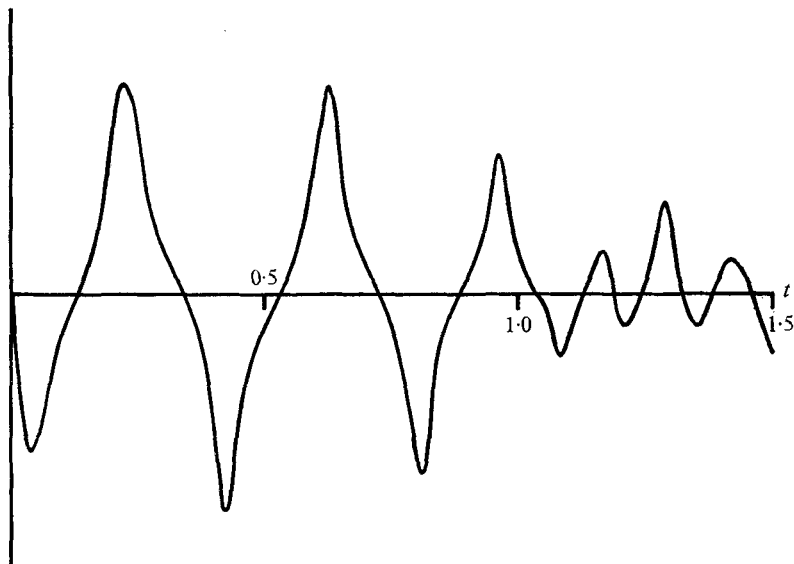


FIGURE 16. Variation of the poloidal flux threading the equator with time for model 2 with  $n = 3$ ,  $P = 100$ .

steady mode to be preferred, then the explanation for the initial oscillatory behaviour of model 3 becomes clear. The prescribed magnetic Reynolds number is initially so far above the critical value that the steady mode is suppressed, and an oscillatory mode excited instead. As this solution grows, the nonlinear effects become important, reducing the magnitude of the  $\alpha$ -effect. In some respects this is equivalent to a reduction in  $R_m$ . Such a reduction would bring the system back into a regime in which the steady mode would be preferred, thus explaining the transition to a steady solution observed in the dipole case. The parallel is not exact, however, since the reduction in the  $\alpha$ -effect due to the Lorentz forces is a function of position, whereas lowering the magnetic Reynolds number reduces the  $\alpha$ -effect by the same factor everywhere. This probably accounts for the failure of the quadrupole solution to make the transition to a steady state.

## 6. Conclusion

The technique pursued in this paper, of treating the dynamo problem as an initial-value problem, has served two main purposes. It has confirmed that the marginally stable modes obtained by solution of the associated eigenvalue problem do indeed occur when the system is perturbed by an arbitrary magnetic field. It has also enabled nonlinear models to be investigated for the first time in a spherical geometry. It appears that under suitable conditions the solution of the nonlinear problem is closely approximated by the linear solution, even at highly supercritical magnetic Reynolds numbers. This fact should inspire confidence in the value of investigating linear kinematic dynamo models.

In some cases, however, the nonlinear models have exhibited features in their

behaviour not observed for linear models. A disappointing but not altogether unexpected shortcoming of these solutions is their failure to give any clue as to the nature of the geomagnetic reversals. The first part of the butterfly diagram for model 2 with  $n = 3$  and  $P = 100$ , shown in figure 13, appears hopeful at first glance, as reversals of the toroidal field occur over a time small compared with the total oscillation period. Unfortunately, this effect is not reflected in the poloidal field, whose time dependence is portrayed in figure 16. Here the value of  $a$  at the point  $(1, \frac{1}{2}\pi)$  has been used as a measure of the poloidal field. This is a different quantity from the dipole moment, which determines the appearance of the external field at large distances. It does, however, give a reasonably good indication of the bulk behaviour of the poloidal field, being proportional to the total magnetic flux threading the equator.

In all the nonlinear models considered, any distortion of the sinusoidal time dependence of the poloidal field predicted by linear theory has been towards a 'spiked' rather than a flattened wave form. It seems almost certain that a full magnetohydrodynamic model involving the effects of the Lorentz forces on the large-scale velocity as well as on the turbulence will be necessary if a realistic model of the earth's dynamo is to be formulated.

The work described in this paper was submitted in partial fulfilment of the requirements for a Ph.D. degree at the University of East Anglia. The author would like to express his gratitude to his research supervisor, Prof. M. B. Glauert, for his helpful advice throughout the course of the work. Thanks are also due to Prof. P. H. Roberts for suggesting the investigation of nonlinear models. The work was financed by an S.R.C. research studentship.

#### REFERENCES

- BRAGINSKIĪ, S. I. 1964 Kinematic models of the earth's hydromagnetic dynamo. *Geomag. Aeron.* **4**, 732. (English trans. p. 572.)
- BULLARD, E. C. & GELLMAN, H. 1954 Homogeneous dynamos and terrestrial magnetism. *Phil. Trans. A* **247**, 213.
- COWLING, T. G. 1933 The magnetic field of sunspots. *Mon. Not. Roy. Astr. Soc.* **94**, 39.
- DU FORT, E. C. & FRANKEL, S. P. 1953 Stability conditions in the numerical treatment of parabolic differential equations. *Math. Tables & Aids to Comp.* **7**, 135.
- GIBSON, R. D. & ROBERTS, P. H. 1969 In *The Application of Modern Physics to the Earth and Planetary Interiors* (ed. S. K. Runcorn), pp. 577–602. Wiley.
- GUBBINS, D. 1972 Kinematic dynamos and geomagnetism. *Nature*, **238**, 119.
- LILLEY, F. E. M. 1970 On kinematic dynamos. *Proc. Roy. Soc. A* **316**, 153.
- MAUNDER, E. W. 1922 The sun and sunspots 1820–1920. *Mon. Not. Roy. Astr. Soc.* **82**, 534.
- MOFFATT, H. K. 1972 An approach to a dynamic theory of dynamo action in a rotating conducting fluid. *J. Fluid Mech.* **53**, 385.
- PARKER, E. N. 1971 The generation of magnetic fields in astrophysical bodies. IV. The solar and terrestrial dynamos. *Astrophys. J.* **164**, 491.
- ROBERTS, P. H. 1972 Kinematic dynamo models. *Phil. Trans. A* **272**, 663.
- ROBERTS, P. H. & STIX, M. 1971 The turbulent dynamo. *N.C.A.R. Tech. Note*, TN/IA-60.
- ROBERTS, P. H. & STIX, M. 1972  $\alpha$ -effect dynamos by the Bullard–Gellman formalism. *Astron. Astrophys.* **18**, 453.

- STEENBECK, M. & KRAUSE, F. 1969 On the dynamo theory of stellar and planetary magnetic fields. I. A.c. dynamos of solar type. *Astronom. Nachr.* **291**, 49. (Trans. in Roberts & Stix 1971.)
- STEENBECK, M., KRAUSE, F. & RÄDLER, K.-H. 1966 A calculation of the mean electromotive force in an electrically conducting fluid in turbulent motion, under the influence of Coriolis forces. *Z. Naturforsch.* **21a**, 369.
- STIX, M. 1972 Nonlinear dynamo waves. *Astron. Astrophys.* **20**, 9.